Article

On the Permeation of Polychlorinated Dibenzodioxins and Dibenzofurans through Lipid Membranes: Classical MD and Hybrid QM/MM-EDA Analysis

Raúl Alvarado,[a] Gustavo Cárdenas,[b] Juan J. Nogueira,[b,c] Nicolás Ramos-Berdullas,[a,*] Marcos Mandado[a,*]

[a]Department of Physical Chemistry, University of Vigo, Lagoas-Marcosende s/n, ES-36310-Vigo, Galicia, Spain.
[b]Department of Chemistry, Universidad Autónoma de Madrid, Calle Francisco Tomás y Valiente, 7, 28049, Madrid, Spain.
[c]IADCHEM, Institute for Advanced Research in Chemistry, Universidad Autónoma de Madrid, Calle Francisco Tomás y Valiente, 7, 28049, Madrid, Spain
* Correspondence: nicolas.ramos@uvigo.es, mandado@uvigo.es

Abstract: The permeation of dioxin-like pollutants, namely, chlorinated dibenzodioxins and dibenzofurans, through lipid membranes has been simulated using classic molecular dynamics (CMD) combined with the umbrella sampling approach. The most toxic forms of chlorinated dibenzodioxin and dibenzofuran, 2,3,7,8-tetrachloro-p-dibenzodioxin (TCDD) and 2,3,7,8-tetrachlorodibenzofuran (TCDF), and a dioleyl-phosphatidylcholine (DOPC) lipid membrane of 50 Å wide have been chosen for our study. The free energy profile shows the penetration process is largely favoured thermodynamically (ΔG≈-12 kcal/mol), with a progressively decrease of the free energy until reaching the energy minima at distances of 8Å and 9.5Å from the centre of the membrane for, respectively, TCDD and TCDF. At the centre of the membrane, both molecules display subtle local maxima with free energy differences of 0.5 and 1 kcal/mol with respect to the energy minima for TCDD and TCDF, respectively. Furthermore, the intermolecular interactions between the molecules and the lipid membrane have been characterized at the minima and the local maxima using hybrid quantum mechanics/molecular mechanics energy decomposition analysis (QM/MM-EDA). Total interaction energies of -17.5 and -16.5 kcal/mol have been found at the energy minima for TCDD and TCDF, respectively. In both cases, the dispersion forces govern the molecule-membrane interactions, no significant changes have been found at the local maxima, in agreement with the classical free energy profile. The small differences found in the results obtained for TCDD and TCDF point out the adsorption and diffusion processes through the cell membrane are not related to the different toxicity shown by these pollutants.

Keywords: dioxins; lipid membranes; molecular dynamics; QM/MM; EDA

1. Introduction

Chlorinated dibenzo-p-dioxins and dibenzofurans (CDDs and CDFs), together with certain polychlorinated biphenyls (PCBs), constitute a family of highly toxic compounds, known as dioxins, whose carcinogenic and mutagenic effects in living organisms are widely known [1-5]. They are considered persistent organic pollutants (POPs) and have an extensive list of production sources, including: incineration of waste, production of iron and steel, chlorine bleaching, sewage sludge or even natural processes such as forest fires, among others [6-8]. Due to their extensive production and high persistence in nature, CDDs and CDFs pose a serious risk for the environmental health. Among the most toxic CDDs and CDFs, the tetrachlorinated forms of 2,3,7,8-tetrachloro-p-dibenzodioxin (TCDD) and 2,3,7,8-tetrachlorodibenzofuran (TCDF) may be remarked [9-10]. Their toxicity has been extensively investigated and have been mainly related to the affinity of dioxins by the AhR (aryl hydrocarbon receptor) cytosolic protein [11-13]. However, their toxicity is also connected to their high bioaccumulation within the fat tissues of living

 doi:10.20944/preprints202211.0283.v1

organisms [14,15], which causes the spread along the food chain by ingestion of animals or plants where they may be present in low concentration [16].

Adsorption and diffusion of dioxins through the cell membrane are the first steps of its action mechanism within cells. The qualitative aspects of this mechanism have been extensively studied experimentally for TCDD, the most toxic dioxin, finding clear evidences that the binding of TCCD to AhR is the key stage that determines the toxicity to a greater extent, as mentioned above. AhR is a transcription factor that regulates the expression of different genes and is related to many disorders and diseases, such: as major depressive disorder, cardiovascular disease, multiple sclerosis, rheumatoid arthritis, asthma, and allergic responses. Upon binding of dioxins to AhR, translocation into the nucleus and dimerization with ARNT (AhR nuclear translocator) may take place, provoking changes in gene transcription [11-13].

Although the qualitative aspects of the action mechanism of dioxins are relatively well-known, the mechanism itself has been scarcely investigated at molecular level [17-19]. Particularly interesting is the adsorption and diffusion processes through the cell membrane and the role played by these membrane processes on the toxic levels detected for each CDD and CDF. Herein, computational simulations using classical methods provide very useful information about the thermodynamics and kinetics of the dioxin dehydration and diffusion steps along the membrane. Subsequent calculations at hybrid quantum mechanics/molecular mechanics (QM/MM) level offer an accurate picture of the intra and intermolecular interactions that regulate the permeation of the membrane to different dioxins. Classical Molecular Dynamics (CMD) simulations of the penetration of TCDD through a lipid membrane have been already performed by Casalegno et al. [19]. They found the hydrophobic nature of TCDD favours its penetration within the structure of the lipid bilayer. A progressive decrease of the free energy profile from the water-lipid interface to the hydrophobic region was found, with a small increase of the free energy at the center of the membrane, leading to a subtle local free energy maximum. They also simulated the penetration of TCDD clusters of up to ten molecules, finding that the adsorption of the cluster molecules takes place sequentially but assisted by the intermolecular interactions among them. However, cluster disaggregation occurs just after adsorption so that TCDD migration across the membrane happens for each molecule independently of the rest.

As for CDFs, and more concretely, TCDF, no theoretical works have been published on its adsorption and membrane permeation or on its affinity for AhR to the best of our knowledge. TCDF presents some important structural and electronic differences with respect to TCDD, such as polarity and a partial reduction of local aromaticity of the phenyl rings, both induced by the replacement of the central dioxin-like ring by a furan-like ring. These structural and electronic differences may change the action mechanism with respect to TCDD, starting by the cell membrane crossing process. In fact, according to the toxic equivalency factors (TEFs), which were developed to account for the relative toxicity of dioxins, TCDD is significantly more toxic than TCDF [20].

Herein, a comparative study of the permeation of TCDD and TCDF molecules through a lipid membrane model has been carried out using umbrella sampling combined with CMD. In order to get more insight into the process and understand the differences found between TCDD and TCDF, a hybrid QM/MM energy decomposition analysis (QM/MM-EDA) has been applied at specific regions along the permeation path (free energy minima and maxima) [21]. This is the first time the permeation of dioxins through biological membranes is studied at quantum mechanical level. Thus, the results presented here serve also to check the ability of classical force fields to represent the intermolecular interactions of these molecules with the lipid bilayer.

2. Methodology

2.1. CMD simulations

 doi:10.20944/preprints202211.0283.v1

The membrane model employed for the CMD simulations consists of a lipid bilayer formed by two leaflet of 64 1,2-dioleyl-sn-glycero-phosphocholine (DOPC) molecules. Each layer is solvated by water molecules with a total thickness of 25 Å on each side. In order to reproduce the physiological concentration of KCl, chlorine anions and potassium cations were added until a concentration of 0.15 M. Casalegno *et al*. [19] employed a similar membrane model for their CMD simulations with a bilayer of 64 molecules each surrounded by water, but using as lipid unit 1,2-dipalmitoyl-sn-glycero-3-phosphocholine (DPPC), whose non-polar region differs slightly from that of DOPC. Phosphatidylcholine is one of the major phospholipid components of the plasma membrane and of the membrane of endoplasmic reticulum, Golgi apparatus, mitochondria, endosomes and lysosomes [22]. Due to the biological relevance of phosphatidylcholine lipids, DOPC and DPPC membranes are widely chosen as model in experimental and computational investigations. DOPC was chosen as lipid unit by our group in previous studies of membrane permeability with very satisfactory results in comparison with the available experimental data [21,23]. The membrane was built with the help of the CHARMM-GUI website [24].

The reference CDD and CDF pollutants included in our study correspond to the more toxic forms, namely the TCDD and TCDF molecules. The molecules were initially placed at a distance of 32 Å along the normal direction from the centre of mass of the membrane with the help of the *tleap* module of AmberTools19 [25], giving rise to a system of 35462 atoms. The Lipid17 force field, an updated version of the Lipid11 [26] and the Lipid14 [27] force fields, was employed to describe the lipid bilayer, whereas the TIP3P model was used to describe the water molecules [28]. K^+ and Cl^- ions were represented by suitable Amber parameters [29]. The intramolecular and Lenard-Jones parameters of TCDD and TCDF were taken from the general Amber force field for organic molecules. To calculate the atomic charges, the geometry of the pollutants was initially optimized at DFT level using the M062X [30] functional and the 6-311G(d,p) basis set, after which the Merz-Singh-Kollman scheme was applied at the same level of theory. CMD simulations were run with the pmemd CUDA implementation [31] of the Amber20 program [25].

Before the simulation of the pollutants' membrane permeability, the equilibration of the structure and density of the solvated lipid bilayer was carried out. Initially, the system was minimized with the steepest descent method for 5000 steps, and the conjugate gradient method for another 5000 steps. Afterwards, it was progressively heated up to 303 K. In a first step, the system was heated to 100 K in the canonical (NVT) ensemble, using a Langevin thermostat with a collision frequency of 1 ps^{-1}. In a second step, the system was heated from 100 K to the desired production temperature of 303 K at constant temperature and pressure (NPT ensemble), using again the Langevin thermostat and, in order to keep the pressure around 1 bar, the Berendsen barostat [32] with a pressure relaxation time of 1 ps. The positions of the lipid bilayer and the TCDD and TCDF molecules were restrained during the heating process by applying force constants of 10 kcal/(mol·Å^2) and 5 kcal/(mol·Å^2), respectively. Once the system temperature reached 303 K, two consecutive MD simulations of 4 ns each were carried out at constant temperature and pressure. During these two simulations the restrictions to the position of the lipid molecules were reduced gradually by decreasing the force constant from 10 kcal/(mol·Å^2) in the first simulation, to 5 kcal/(mol·Å^2) in the second one. The force constant for the pollutants was kept at 5 kcal/(mol·Å^2). As final step in the equilibration process, a 100 ns production simulation was carried out in the NPT ensemble, keeping again the restrain force constant of the pollutants at 5 kcal/(mol·Å^2) but removing the restrictions for the lipid positions.

Once the system was equilibrated, the permeation processes of TCDD and TCDF through the lipid bilayer were simulated by means of the umbrella sampling technique. The distance between the centres of mass of the pollutant and membrane along the z axis (perpendicular to the lipid bilayer) was defined as reaction coordinate (see Figure 1), so that a value of 0 Å corresponds to the situation where the pollutant is located at centre of the membrane. A distance of 32.0 Å from the centre was taken as the initial value of the reaction coordinate. The whole reaction coordinate was divided into 65 windows of 0.5 Å

Preprints (www.preprints.org) | NOT PEER-REVIEWED | Posted: 15 November 2022 doi:10.20944/preprints202211.0283.v1

width each. A CMD simulation of 20 ns was run within each window using the NPT ensemble. The initial geometry and velocities for a given window were taken from the last snapshot of the previous one. Additionally, a harmonic bias potential with a force constant of 2.5 kcal/(mol·Å^2) was applied on the reaction coordinate. Thus, the full simulation of the pollutants penetration from the aqueous phase to the centre of the membrane took 1300 ns. The parameters employed for the simulation of each window were the same as those employed for the 100 ns production described above. The Weighted Histogram Analysis Method (WHAM) was employed to obtain the free-energy profiles [33]. During the full protocol, the particle-mesh Ewald method with a grid spacing of 1.0 Å was used to compute the electrostatic interactions, and a 10 Å cutoff for the nonbonded interactions was chosen. Moreover, the bonds involving hydrogen atoms were restrained by the SHAKE algorithm [34], and a time step of 2 fs was used.

2.2. QM/MM-EDA calculations

The interaction energy, E_{int}, between two molecular systems A and B is defined as,

$$E_{\text{int}} = E_{\text{AB}} - (E_{\text{A}}^{\text{AB}} - E_{\text{B}}^{\text{AB}}) \quad (1)$$

where E_{AB} refers to the energy of the complex and E_{A}^{AB} and E_{B}^{AB} to the energies of the isolated systems calculated in the same geometry and with the same basis set as they have in the complex.

The EDA scheme applied in this work for the study of non-covalent interactions is based on the partition of the complex energy, formulated in terms of the 1-electron density and density matrix and the exchange-correlation density (Eq (2)), into perturbed and unperturbed terms.

$$E_{\text{AB}} = -\frac{1}{2}\int \nabla^2 \rho(\mathbf{r},\mathbf{r}')_{\mathbf{r}'=\mathbf{r}}\, \mathrm{d}\mathbf{r} + \int \hat{\mathbf{v}}_{\text{N}}(\mathbf{r})\,\rho(\mathbf{r})\mathrm{d}\mathbf{r} + \frac{1}{2}\int\int \frac{\rho(\mathbf{r}_1)\rho(\mathbf{r}_2)}{|\mathbf{r}_2-\mathbf{r}_1|}\mathrm{d}\mathbf{r}_1\mathrm{d}\mathbf{r}_2 + \\ + \frac{1}{2}\int\int \frac{\rho_{\text{XC}}(\mathbf{r}_1,\mathbf{r}_2)}{|\mathbf{r}_2-\mathbf{r}_1|}\mathrm{d}\mathbf{r}_1\mathrm{d}\mathbf{r}_2 + \sum_{I=1}^{N}\sum_{J>I}^{N}\frac{Z_I Z_J}{|\mathbf{R}_I-\mathbf{R}_J|} \quad (2)$$

In Eq (1), $\rho(\mathbf{r})$ and $\rho(\mathbf{r},\mathbf{r}')_{\mathbf{r}'=\mathbf{r}}$ represent the 1-electron density and density matrix, respectively, $\rho_{\text{XC}}(\mathbf{r}_1,\mathbf{r}_2)$ the exchange-correlation density, $\hat{\mathbf{v}}_{\text{N}}(\mathbf{r})$ the nuclei potential operator, **r** and **R** the electron and nuclei positions, respectively, and Z_I and Z_J the atomic numbers. The different unperturbed terms correspond to E_{A}^{AB} and E_{B}^{AB} whereas the perturbed ones to E_{int}. Since the mathematical formulation of this EDA scheme has been extensively explained elsewhere, only the most relevant aspects will be reviewed here [35,36]. The way to define the unperturbed and perturbed energy terms is through the introduction of the deformation densities associated with the intermolecular interaction. Thus, the 1-electron density, the density matrix and the exchange-correlation density of Eq (2) can be expressed as a sum of the densities of the isolated A and B systems plus the deformation densities induced by the Pauli repulsion (Pau) and polarization (Pol).

$$\rho(\mathbf{r}) = \rho_{\text{A}}(\mathbf{r}) + \rho_{\text{B}}(\mathbf{r}) + \Delta\rho_{\text{Pau}}(\mathbf{r}) + \Delta\rho_{\text{Pol}}(\mathbf{r}) \quad (3)$$

$$\rho(\mathbf{r},\mathbf{r}') = \rho_{\text{A}}(\mathbf{r},\mathbf{r}') + \rho_{\text{B}}(\mathbf{r},\mathbf{r}') + \Delta\rho_{\text{Pau}}(\mathbf{r},\mathbf{r}') + \Delta\rho_{\text{Pol}}(\mathbf{r},\mathbf{r}') \quad (4)$$

$$\rho_{\text{XC}}(\mathbf{r}_1,\mathbf{r}_2) = \rho_{\text{XC,A}}(\mathbf{r}_1,\mathbf{r}_2) + \rho_{\text{XC,B}}(\mathbf{r}_1,\mathbf{r}_2) + \rho_{\text{X,AB}}(\mathbf{r}_1,\mathbf{r}_2) + \Delta\rho_{\text{XC}}(\mathbf{r}_1,\mathbf{r}_2) \quad (5)$$

Preprints (www.preprints.org) | NOT PEER-REVIEWED | Posted: 15 November 2022 doi:10.20944/preprints202211.0283.v1

The intermolecular electron exchange in Eq (4), $\rho_{X,AB}(\mathbf{r}_1,\mathbf{r}_2)$, occurs before the polarization of the A and B systems and gives rise to the intermolecular exchange term of the Pauli energy. On the other hand, $\Delta\rho_{XC}(\mathbf{r}_1,\mathbf{r}_2)$ represents the polarization of the exchange-correlation density. By introducing Eqs (3), (4) and (5) in Eq (2) and partitioning the nuclei potential operator into $\hat{\mathbf{v}}_{N_A}(\mathbf{r})$ and $\hat{\mathbf{v}}_{N_B}(\mathbf{r})$ and the nuclear repulsion energy into intramolecular and intermolecular terms, the unperturbed energy terms can be easily identified and removed from Eq (2), leaving only the perturbed terms that account for the total interaction energy. Moreover, these perturbed terms can be grouped into contributions with different physical meaning: electrostatic (elec), exchange (exc), repulsion (rep) and polarization (pol).

$$E_{int} = E_{elec} + E_{exch} + E_{rep} + E_{pol} \quad (6)$$

The sum of exchange and repulsion energies in Eq (6) gives rise to the Pauli (Pau) energy.

For weak intermolecular interactions, a 2nd order perturbation scheme allows splitting the polarization energy into dispersion (disp) and induction (ind) [36], giving rise to the traditional interaction energy perturbational partitioning scheme.

$$E_{int} = E_{elec} + E_{Pau} + E_{ind} + E_{disp} \quad (7)$$

When a QM/MM electrostatic embedding is introduced in the calculations, the electrostatic potential, $\hat{\mathbf{V}}_{MM}(\mathbf{r})$, associated with the MM charges, q_i,

$$\hat{\mathbf{V}}_{MM}(\mathbf{r}) = \sum_{i=1}^{NA_{MM}} \frac{q_i}{|\mathbf{r}-\mathbf{R}_i|} \quad (8)$$

must be added to both or one of the nuclei potential operators, $\hat{\mathbf{v}}_{N_A}(\mathbf{r})$ and $\hat{\mathbf{v}}_{N_B}(\mathbf{r})$, as well as to the nuclear repulsion energy in order to get the energy decomposition of Eq (7) at QM/MM level of theory. This QM/MM-EDA scheme is applied here.

In the study of the membrane-pollutant interactions, the system has been split into two subsystems, the pollutant molecule (A) and the DOPC membrane plus the water molecules and the K^+ and Cl^- (B). As will be explained in the next section, the QM region includes the pollutant and a minimum of seven DOPC molecules, while the remaining atoms are included in the MM region and interact with the atoms of the QM layer by an electrostatic embedding approach. Thus, the subsystem A is fully described at QM level, whereas the complex and the subsystem B are described at QM/MM level. In our particular case, $\hat{\mathbf{V}}_{MM}(\mathbf{r})$ has been added to $\hat{\mathbf{v}}_{N_B}(\mathbf{r})$ and to the nuclear term of the electrostatic energy, E_{elec}^{Nuc}, as follows,

$$\hat{\mathbf{v}}_{N_B}^{QM/MM}(\mathbf{r}) = \mathbf{v}_{N_B}(\mathbf{r}) + \hat{\mathbf{V}}_{MM}(\mathbf{r}) \quad (9)$$

$$E_{elec}^{Nuc} = \sum_{I=1}^{N_A}\sum_{J=1}^{N_B} \frac{Z_I Z_J}{|\mathbf{R}_I - \mathbf{R}_J|} + \sum_{I=1}^{N_A} \int Z_I \hat{\mathbf{V}}_{MM}(\mathbf{r})\delta(\mathbf{R}_J - \mathbf{r})\,d\mathbf{r} \quad (10)$$

The Gaussian16 software package [37] has been employed for the QM/MM calculations. Electron densities in the QM region have been obtained using density functional theory (DFT), with the M062X functional and the 6-31G(d,p) basis set. This is an appropriate functional to describe non-covalent interactions without the introduction of empirical dispersion corrections. To apply the QM/MM-EDA scheme explained above, three different electronic structure calculations are required; one for the complex (pollutant+solvated

 doi:10.20944/preprints202211.0283.v1

membrane), one for the solvated membrane and another one for the pollutant molecule. The Gaussian input files for these calculations have been automatically generated with the MoBioTools package [38,39]. Both the pollutant and membrane input files include the full complex basis set in order to avoid the basis set superposition error in the QM region. As mentioned above, the QM/MM calculations were done using an electrostatic embedding. Therefore, both the complex and membrane input files include the atomic charges of the MM region, which, together with the corresponding Cartesian coordinates, have been read from the Amber CMD simulations and written to the Gaussian input files using MoBioTools. The calculations of the interaction energy, its different components and the analysis of the deformation densities have been done with the EDA-NCI program [40].

3. Results and Discussion

As mentioned in the previous section, the permeation of pollutants through the membrane has been simulated using CMD combined with the umbrella sampling technique. The free energy profiles obtained by the WHAM from the simulations performed separately for TCDD and TCDF molecules are shown in Figure 1, together with a scaled schematic representation of the DOPC bilayer. The simulation has been done only for the left side of the path, from -35 Å to the centre of the membrane. Then, the free energy profile has been replicated on the right side of the plot in order to show the energy minima of the pollutants on different sides of the membrane.

The TCDD and TCDF energy profiles are very similar. The hydrophobic nature of the pollutants favours the permeation through the lipid bilayer with a progressive decrease of the free energy from the water-lipid interface to the hydrophobic region. Moreover, a small increase of the free energy at the centre of the membrane is found in both cases, leading to subtle local free energy maxima. These profiles are in agreement with the CMD simulation performed by Casalegno et al for the permeation of a TCDD molecule through a DPPC membrane. They found the free energy minimum around 10 Å from the centre of the bilayer, whereas our minimum is located around 8.0 Å. The energy well obtained by Casalegno et al at the free energy minimum was around -10.3 kcal/mol, whereas the energy well obtained here is -11.8 kcal/mol. On the other hand, the free energy difference between the local maximum found at the centre of the membrane and the minimum was found to be around 1.7 kcal/mol in reference [19], whereas it is only 0.7 kcal/mol in this work. These small differences can be related to the slightly different membranes employed and, of course, to differences in the technical details related to the setup and the CMD simulations.

Looking now at the differences between TCDD and TCDF, the free energy minimum in the latter shows a small displacement with respect to the minimum of TCDD and it is located at 9.0 Å (and not at 8.0 Å) from the centre of the membrane. On the other hand, the free energy profile in the hydrophobic region of the lipid bilayer is slightly above the TCDD profile. The free energy minimum and the local maximum of TCDF are -11.2 and -10.4 kcal/mol, respectively, which are around 0.7 kcal/mol less negative than those obtained for TCDD. In other words, the permeation of TCDF is lowly less favourable than that of TCDD. This slight displacement to the hydrophilic region and slight destabilization inside the lipid bilayer with respect to TCDD could be explained by the small polar character of TCDF, with a calculated dipole moment of 0.59 D.

Preprints (www.preprints.org) | NOT PEER-REVIEWED | Posted: 15 November 2022 doi:10.20944/preprints202211.0283.v1

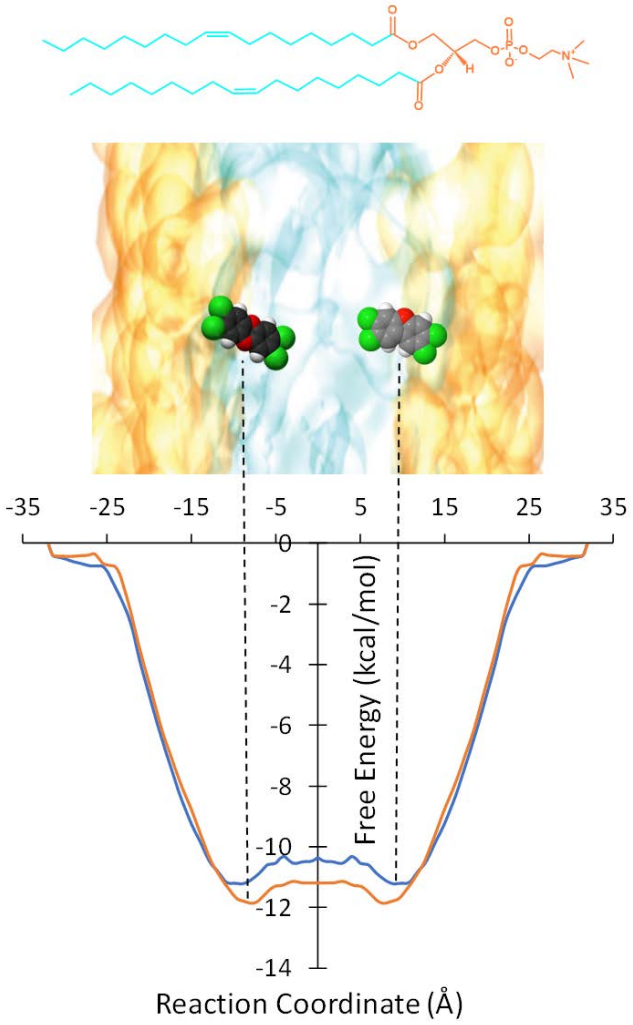

Figure 1. Top: Schematic representation of the TCDD and TCDF molecules embedded in a DOPC lipid bilayer. The polar and non-polar regions of the lipid bilayer are represented in orange and cyan, respectively. Bottom: Free energy profiles of the TCDD (red line) and TCDF (blue line) permeation processes through the lipid bilayer. The free energy minima are indicated by vertical dashed lines.

In order to shed more light on the driving forces responsible of the TCDD and TCDF permeation and the slight differences encountered between them, an energy analysis of the intermolecular interactions between these molecules and the DOPC lipids has been performed around the free energy minima. This analysis could be performed by relying in the energy provided by the force field [21]. However, more accurate conclusions can be extracted if a QM/MM scheme is employed in the calculation and decomposition of the interaction energy, as was recently done for the permeation of cisplatin through a DOPC bilayer [21]. This accurate analysis requires the description of the interaction region using a QM level, but also the description of the environment effects with a classical approach. As explained in Section 2, a hybrid QM/MM method including DFT for the QM region and an electrostatic embedding for the MM region has been employed here to calculate the interaction energies. Subsequently, the electrostatic, Pauli, induction and dispersion components of the interaction energy have been obtained with the QM/MM-EDA scheme described also in Section 2. The first step is to obtain the optimal size of the QM region for the QM/MM calculations. In our case, the optimal QM region must contain the pollutant and the minimum number of DOPC molecules (N_{min}) necessary to get the pollutant-lipid total interaction energy and its different components converged with the region size. In

Preprints (www.preprints.org) | NOT PEER-REVIEWED | Posted: 15 November 2022 doi:10.20944/preprints202211.0283.v1

order to obtain N_{min}, one arbitrary snapshot has been selected around the free energy minimum of the CMD simulations of TCDD and TCDF permeation. Then, using these two geometries from these snapshots as input, QM/MM-EDA calculations have been performed for QM regions of increasing number of DOPC molecules (N).

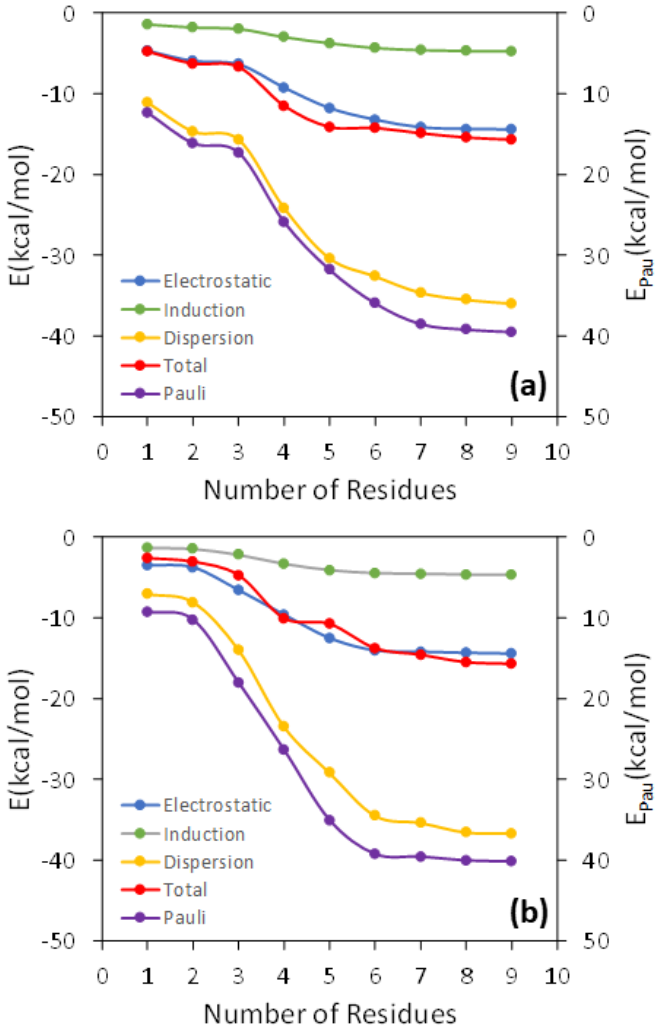

Figure 2. Analysis of the convergence of the interaction energy and its different components as the number of the DOPC molecules increases in the QM region for an arbitrary geometry around the free energy minima of the TCDD (**a**) and TCDF (**b**) permeation.

In Figure 2, the total interaction energy as well as the electrostatic, Pauli, induction and dispersion energies are represented against N for the interaction of TCDD and TCD F with the lipid bilayer. As can be observed, all the energy terms are converged within the interval of ±1 kcal/mol for N=7, both in the case of TCDD and TCDF. It is remarkable that a slower convergence is not found for the electrostatic and induction energies. These terms correspond to the interactions with largest range, and it could be expected that they need a larger number of DOPC molecules to converge than the shortest range Pauli and dispersion energies. This occurs, for instance, in solvated anions, such as ammonium cation, formate anion and the zwitterionic form of glycine [41]. However, this is not the case for the interaction of TCDD and TCDF with the lipid bilayer since the convergence is reached almost at the same time for all the energy terms. On the other hand, this result does not confront with the general assumption that Pauli energy is a short-range interaction. This character is clearly reflected on the magnitude of the Pauli deformation density, $\Delta\rho_{Pau}$, which is represented using different density cut-offs and compared with the polarization

Preprints (www.preprints.org) | NOT PEER-REVIEWED | Posted: 15 November 2022 doi:10.20944/preprints202211.0283.v1

density, $\Delta\rho_{Pol}$, in Figure 3. As it can be observed, $\Delta\rho_{Pol}$ spreads over a larger region than $\Delta\rho_{Pau}$ when the same cut-off is applied. $\Delta\rho_{Pol}$ is involved in the calculation of induction and dispersion energies, whereas $\Delta\rho_{Pau}$ only enters into the calculation of the repulsive part of the Pauli energy. The unexpected slow convergence of the Pauli and dispersion energies with the number of DOPC molecules may be related with the large contribution of these terms to the total interaction energy in comparison with the induction and electrostatic energies (see Figure 2). In fact, the dispersion energy is the strongest contribution among the attractive interactions for the two pollutants. This is in contrast to the solvated ions where the electrostatic energy is the dominant term in the interaction of the ion with the solvent [41].

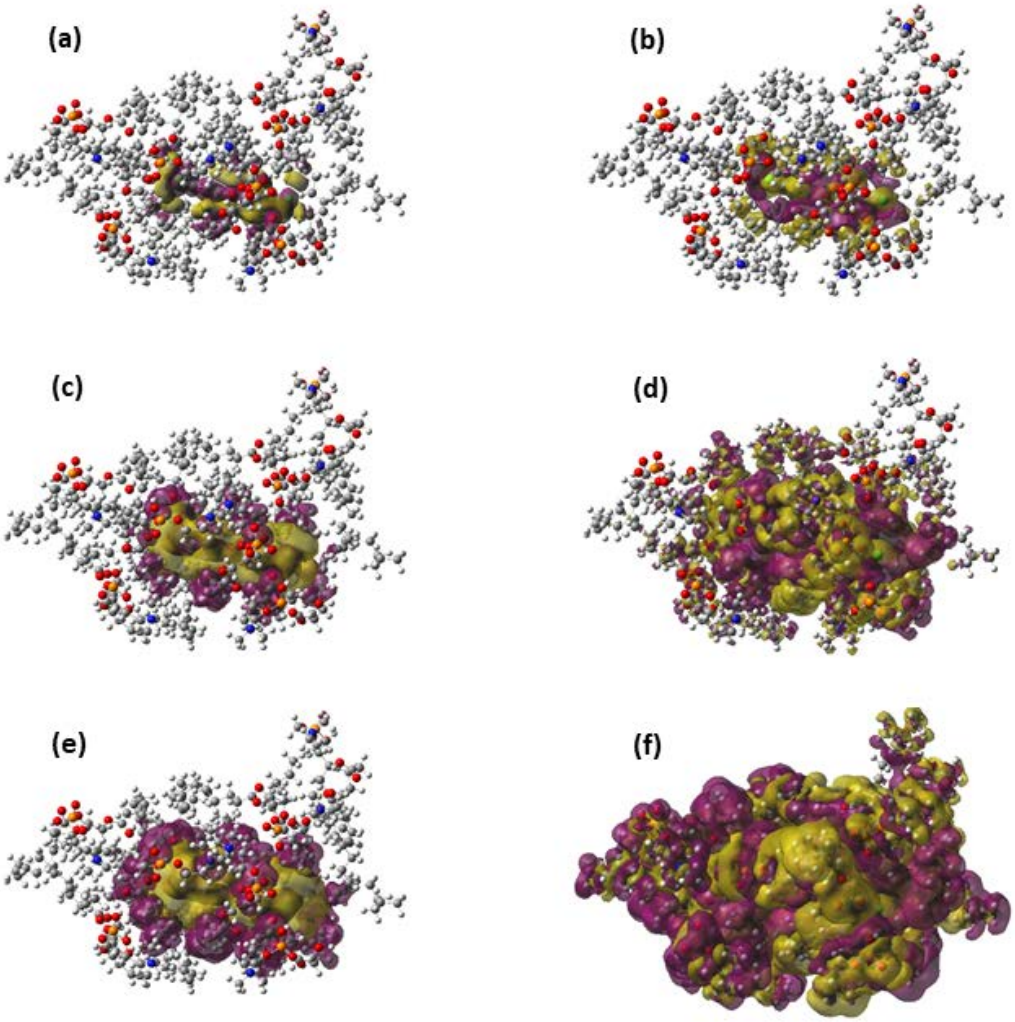

Figure 3. Representations of the Pauli deformation density (**a**, **c** and **e**) and the polarization density (**b**, **d** and **f**) for an arbitrary geometry around the free energy minimum of the TCDD permeation. The representation includes only the TCDD molecule and the seven DOPC molecules included in the QM region. The following density cut-offs have been used: 10^{-4} (**a** and **b**), 10^{-5} (**c** and **d**) and 10^{-6} (**e** and **f**).

Once N_{min} has been set to 7, QM/MM-EDA calculations have been carried out at the free energy minima and local maxima at the centre of the bilayer by sampling 100 geometries from each region from the previous CMD simulations. In a recent work on the cisplatin permeation through the same lipid membrane, it was found that the mean values

 doi:10.20944/preprints202211.0283.v1

for the different interaction energy components were relatively well converged after considering 100 geometries. Taking into account the large computational cost of the QM/MM calculations performed here with a QM region size containing 988 atoms, we have selected 100 geometries equally spaced along the corresponding window for the QM/MM-EDA statistics.

The mean values obtained for the total interaction energy and its components at the energy minima and local maxima are collected in Table 1. As it can be observed, the energies obtained at QM/MM level also predict TCDD is slightly more stable within the membrane than TCDF, in agreement with the classical free energy profile. In fact, the interaction energy difference is 1 kcal/mol, almost the same difference found for the free energies obtained classically in the dynamic study. Here, it should be recalled that the geometries used for the quantum mechanical study are those obtained classically as a QM/MM MD sampling is computationally unfeasible. Thus, possible differences arising from changes in the geometrical disposition of the pollutants within the lipid bilayer when going from a classical to the QM/MM MD sampling protocol are not accounted for by our calculations. However, it is remarkable the good correspondence between classical free energies and QM/MM interaction energies, both in absolute and relative terms. Differences in the total values can be mainly ascribed to entropic terms and thermal effects, which are not included in the interaction energies. Anyway, the entropic contribution to the pollutant permeation is expected to be destabilizing, which is also reflected on the positive difference between classical free energies (-11.8 kcal/mol for TCDD and -11.2 kcal/mol for TCDF) and QM/MM interaction energies (-17.5 kcal/mol for TCDD and -16.5 kcal/mol for TCDF). As shown in Table 1, the stabilization of the pollutants within the membrane is clearly associated with the dispersion forces, which is the expected result taking into account the nonpolar (TCDD) or slightly polar (TCDF) character of these molecules and their hydrophobic nature. However, although the electrostatic energy is less than half of the dispersion energy, it is not negligible. This may be due to the large-range character of this energy contribution and the relative proximity of the polar heads of the lipid molecules and the C-O polar bonds of the dioxin and dibenzofuran rings.

The EDA results obtained for the local maximum at the centre of the membrane reflect negligible differences with respect to the minimum for TCDF. The interaction energy difference with respect to the minimum is 1.5 kcal/mol in good agreement with the differences in the classical free energies of 0.7 kcal/mol. According to the results obtained for the different energy components, the slightly higher energy of the local maximum in TCDF arises from the Pauli and induction energies, which increases 2.0 and 0.4 kcal/mol, respectively, with respect to the minimum, which is not compensated by the decrease of the dispersion energy of 0.8 kcal/mol and the unchanged electrostatic contribution. On the contrary, an interaction energy increase of 3.5 kcal/mol with respect to the minimum is found for TCDD. Curiously, all the energy terms decrease (in absolute value) significantly in this case. The percentages of change with respect to the minimum are shown in Table 1. From these percentages, it can be extracted that the largest relative changes with respect to the minimum in TCDD are found in the electrostatic and induction energies. The relative changes in the Pauli repulsion and dispersion are clearly smaller. Thus, the decreases in the Pauli energy when going from the minimum to the maximum (around 8 kcal/mol) is surpassed by the decrease of all the attractive contributions (mainly electrostatic and induction). On the other hand, the energy increase in the total interaction energy is significantly larger than that predicted by the CMD simulation. This could be caused by two reasons: (i) the force field performs bad when describing the interaction between TCDD and the membrane or (ii) there are important entropic effects which are not described by the QM/MM calculations.

Preprints (www.preprints.org) | NOT PEER-REVIEWED | Posted: 15 November 2022 doi:10.20944/preprints202211.0283.v1

Table 1. Mean values of the interaction energy and its different components at the free energy minima and local maxima of the TCDD and TCDF permeation. The percentage of change with respect to the minimum of the energies at the local maximum are given in parenthesis.

Min	Electrostatic	Pauli	Induction	Dispersion	Total
TCDD	-19.6	49.7	-6.5	-41.1	-17.5
TCDF	-19.3	52.1	-6.4	-43.0	-16.5
Max	**Electrostatic**	**Pauli**	**Induction**	**Dispersion**	**Total**
TCDD	-15.0(23.5)	41.2(17.1)	-4.7(27.7)	-35.5(13.6)	-14.0
TCDF	-19.3(0.0)	54.1(3.8)	-6.0(6.3)	-43.8(1.9)	-15.0

The probability distributions of the total interaction energies and its energy components for TCDD and TCDF are depicted in Figure 4. They are only shown for the minima; the local maxima display basically the same profile. It can be observed that the distributions of the energy components present different broadness, whereas no significant differences are found between the pollutants. The broadness of the distributions seems to be associated with the magnitude of the average value, as previously found for the interaction of cisplatin with the same membrane. The maxima of the distributions correspond to the mean values collected in Table 1. As it can be seen, all the energy components but induction are significantly broad. This fact highlights the importance of performing a good sampling protocol when calculating the interaction energies for large systems, instead of relying on an arbitrary configuration of a local potential energy minimum.

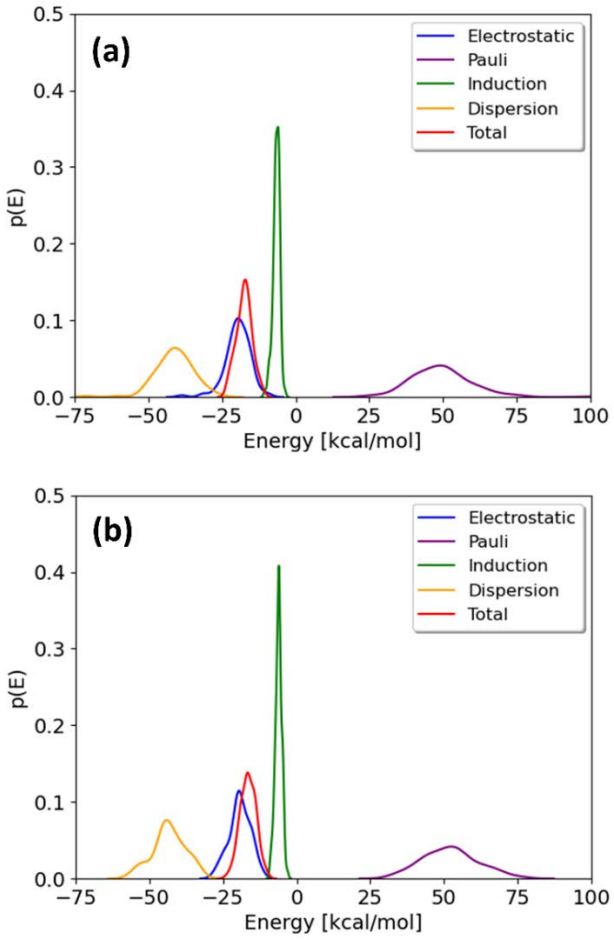

Figure 4. Distributions of the interaction energy and its different components on 100 geometries selected from the free energy minima of the TCDD (**a**) and TCDF (**b**) permeation.

 doi:10.20944/preprints202211.0283.v1

4. Conclusions

In this work, a comparative study of the permeation of TCDD and TCDF pollutants through a lipid membrane formed by DOPC molecules has been carried out using umbrella sampling CMD simulations and a QM/MM-EDA scheme. After the optimization of the QM region size, the QM/MM-EDA study has been performed on a statistical sample of geometries selected from the minima and local maxima regions of the free energy profile obtained from the CMD simulations.

The CMD results show the permeation of TCDF is thermodynamically slightly favoured over TCDD, with no significant free energy difference (around 1 kcal/mol) and a slight displacement of the free energy minimum of TCDF to the hydrophilic region of the membrane with respect to TCDD. Both free energy profiles display also a local energy maximum at the centre of the membrane. The free energy differences with respect to the minimum are small in both cases (around 1 kcal/mol), a fact which reflects that the CMD simulations predict small changes in the lipid-pollutant interactions when crossing the hydrophobic region of the membrane or a compensation between the attractive and repulsive energy changes.

The optimal QM region size for the QM/MM-EDA study was found to be composed by the pollutant molecule and 7 DOPC molecules. The results obtained at QM/MM level are in good agreement with the CMD simulations. Thus, the total pollutant-membrane interaction energy at the minima indicate TCDD is more stable than TCDF by only 1 kcal/mol. However, the calculated QM/MM interaction energies are more negative than the free energies obtained classically, which could be associated with unfavourable entropic or thermal effects inside the membrane, which are taken into account in the classical simulations but not in the QM/MM interaction energy computations. The interaction energy calculated at the centre of the membrane for TCDF and TCDD displays differences with respect to the minimum only a bit larger than those obtained for the classical free energy, another proof of the good correspondence between classical and QM/MM calculations.

The analysis of the different interaction energy components reflects that the stabilization of the pollutants within the hydrophobic region of the membrane is mainly due to a strong dispersion interaction. In both pollutants, dispersion is more than twice the electrostatic energy, whereas the induction energy has a marginal contribution. On the other hand, the Pauli repulsion is also strong, largely compensating the attractive energy terms. The higher interaction energy at the centre of the membrane has a different origin for TCDF and TCDD. In TCDD, a slight increase in the Pauli repulsion energy seems to be the main factor. On the contrary, all the terms decrease (in absolute value) with respect to the minimum in TCDD, being the significant reduction of electrostatic and induction energies, which are proportionally larger than Pauli and dispersion, the reason of the small destabilization of TCDD at the membrane centre with respect to the minimum.

As general conclusion, the small differences encountered between the TCDD and TCDF permeation processes, both in the CMD simulations and the QM/MM-EDA calculations, points out that the adsorption and diffusion steps through the cell membrane do not explain the different toxicity measured for TCDD and TCDF.

Acknowledgments: M.M. and N.R-B. thank Xunta de Galicia for financial support through the project GRC2019/24. N.R-B. thanks Xunta de Galicia for a postdoctoral grant. J.J.N. thanks Comunidad de Madrid through the Attraction of Talent Program (Grant Ref. 2018-T1/BMD- 10261) and the Spanish Ministry of Science and Innovation through the project PID2020-117806GA-I00 funded by MCIN/AEI/10.13039/501100011033

References

1. Polychlorinated dibenzo-para-dioxins and dibenzofurans. *Environ. Health Criteria*. **1989**, *88*, 1.
2. Polychlorinated Dibenzo-para-dioxins and Polychlorinated Dibenzofurans. *IARC Monogr. Eval. Carcinog. Risks Hum. Suppl*. **1997**, *69*, 1.
3. Schecter, A. (Ed), Dioxin and Health, Plenum Press. Springer. New York, USA **1994**.
4. Steenland, K.; Bertazzi, P.; Baccarelli, A.; Kogevinas, M.; Dioxin revisited: developments since the 1997 IARC classification of dioxin as a human carcinogen. *Environ. Health Perspect*. **2004**, *112*, 1265.
5. Biswas, G.; Srinivasan, S.; Anandatheerthavarada, H. K.; Avadhani, N. G. Dioxin-mediated tumor progression through activation of mitochondria-to-nucleus stress signaling. *Proc. Natl. Acad. Sci. U. S. A.* **2008**, *105*, 186.
6. Rappe, C.; Dioxin, Patterns and Source Identification. *Fresenius J. Anal. Chem*. **1994**, *348*, 63.
7. Beck, H.; Droß, A.; Eckart, K.; Mathar, W.; Wittkowski, R. PCDDs, PCDFs and related compounds in paper products. *Chemosphere*. **1989**, *19*, 655.
8. Wiberg, K.; Lundström, K.; Glas, B.; Rappe, C. PCDDs and PCDFs in consumers' paper products. *Chemosphere*. **1989**, *19*, 735.
9. Van Den Berg, M.; Birnbaum, L.; Bosveld, A. T. C.; Brunström, B.; Cook, P.; Feeley, M.; Giesy, J. P.; Hanberg, A.; Hasegawa, R.; Kennedy, S. W.; Kubiak, T.; Larsen, J. C.; Van Leeuwen, F. X. R.; Liem, A. K. D.; Nolt, C.; Peterson, R. E.; Poellinger, L.; Safe, S.; Schrenk, D.; Tillitt, D.; Tysklind, M.; Younes, M.; Wærn, F.; Zacharewski, T. Toxic equivalency factors (TEFs) for PCBs, PCDDs, PCDFs for humans and wildlife. *Environ. Health Perspect.* **1998**, *106*, 775.
10. Van den Berg, M.; Birnbaum, L.; Denison, M.; De Vito, M.; Farland, W.; et al. The 2005 World Health Organization reevaluation of human and Mammalian toxic equivalency factors for dioxins and dioxin-like compounds. *Toxicol. Sci.* **2006**, *93*, 223.
11. Whitlock, J. P. Mechanistic aspects of dioxin action. *Chem. Res. Toxicol.* **1993**, *6*, 754.
12. Mimura J.; Fujii-Kuriyama, Y. Functional role of AhR in the expression of toxic effects by TCDD. *Biochim. Biophys. Acta*, **2003**, *1619*, 263.
13. Denison, M. S.; Soshilov, A. A.; He, G.; DeGroot, D. E.; Zhao, B. Exactly the same but different: promiscuity and diversity in the molecular mechanisms of action of the aryl hydrocarbon (dioxin) receptor. *Toxicol. Sci.* **2011**, *124*, 1.
14. Merrill, M. L.; Emond, C.; Kimi, M. J.; Antignaci, J.-P.; Bizeci, B. L.; Birnbaum, K. C. L. S.; Barouki, R. Toxicological function of adipose tissue: focus on persistent organic pollutants. *Environ. Health Perspect.* **2013**, *121*, 162.
15. Regnier, S. M.; Sargis, R. M. Adipocytes under assault: environmental disruption of adipose physiology. *Biochim. Biophys. Acta, Mol. Basis Dis.* **2014**, *1842*, 520.
16. Schrenk, D.; Chopra, M.; *Dioxins and Polychlorinated Biphenyls in Foods. In Chemical Contaminants and Residues in Food, Woodhead Publishing Series in Food Science, Technology and Nutrition*, D. Schrenk, A. Cartus (eds), Elsevier. Cambridge, USA **2017**.
17. Casalegno, M.; Raos, G.; Sello, G. Identification of viable TCDD access pathways to human AhR PAS-B ligand binding domain. *J. Mol. Graph. Mod*. **2021**, *105*, 107886.
18. Casalegno, M.; Raos, G.; Sello, G. From dioxin to dioxin congeners: understanding the differences in hydrophobic aggregation in water and absorption into lipid membranes by means of atomistic simulations. *Phys. Chem. Chem. Phys.* **2016**, *18*, 1773.
19. Casalegno, M.; Raos, G.; Sello, G. Hydrophobic aggregation and collective absorption of dioxin into lipid membranes: insights from atomistic simulations. *Phys. Chem. Chem. Phys.* **2015**, *17*, 2344.
20. Safe, S. Polychlorinated biphenyls (PCBs), dibenzo-p-dioxins (PCDDs), dibenzofurans (PCDFs), and related compounds: environmental and mechanistic considerations which support the development of toxic equivalency factors (TEFs). *Crit Rev Toxicol.* **1990**, *21*, 51.

21. Cárdenas, G._Pérez-Barcia, A.; Mandado, M.; Nogueira, J. J. Characterization of cisplatin/membrane interactions by QM/MM energy decomposition analysis. *Phys. Chem. Chem. Phys.* **2021**, *23*, 20533.
22. van Meer, G.; de Kroon, A. I. P. M. Lipid map of the mammalian cell. J. *Cell Sci.* **2011**, *124*, 5.
23. Ruano, L.; Cárdenas, G.; Nogueira, J. J. The Permeation Mechanism of Cisplatin Through a Dioleoylphosphocholine Bilayer. *ChemPhysChem* **2021**, *22*, 1.
24. Jo, S.; Kim, T.; Iyer, V. G.; Im, W. CHARMM-GUI: A web-based graphical user interface for CHARMM. *J. Comput. Chem.* **2008**, *29*, 1859.
25. Case, D. et al. AMBER 2020. **2020**,
26. Skjevik, Å. A.; Madej, B. D.; Walker, R. C.; Teigen, K. LIPID11: A Modular Framework for Lipid Simulations Using Amber. *J. Phys. Chem. B* **2012**, *116*, 11124.
27. Dickson, C. J.; Madej, B. D.; Skjevik, Å. A.; Betz, R. M.; Teigen, K.; Gould, I. R.; Walker, R. C. Lipid14: The Amber Lipid Force Field *J. Chem. Theory Comput.* **2014**, *10*, 865.
28. Jorgensen, W. L.; Chandrasekhar, J.; Madura, J. D.; Impey, R. W.; Klein, M. L. Comparison of Simple Potential Functions for Simulating Liquid Water *J. Chem. Phys.* **1983**, *79*, 926.
29. Li, P.; Song, L. F.; Merz, K. M. Systematic Parameterization of Monovalent Ions Employing the Nonbonded Model *J. Chem. Theory Comput.* **2015**, *11*, 1645.
30. Zhao Y.; Truhlar, D. G. The M06 suite of density functionals for main group thermochemistry, thermochemical kinetics, noncovalent interactions, excited states, and transition elements: two new functionals and systematic testing of four M06-class functionals and 12 other functionals. *Theor. Chem. Acc.,* **2008**, *120*,215.
31. Salomon-Ferrer, R.; Götz, A. W.; Poole, D.; Le Grand, S.; Walker, R. C. Routine Microsecond Molecular Dynamics Simulations with AMBER on GPUs. 2. Explicit Solvent Particle Mesh Ewald. *J. Chem. Theory Comput.* **2013**, *9*, 3878.
32. Berendsen, H. J. C.; Postma, J. P. M.; van Gunsteren, W. F.; DiNicola, A.; Haak, J. R. Molecular dynamics with coupling to an external bath. *J. Chem. Phys.* **1984**, *81*, 3684.
33. a) Kumar, S.; Rosenberg, J. M.; Bouzida, D.; Swendsen, R. H.; Kollman, P. A. The weighted histogram analysis method for free-energy calculations on biomolecules. I. The method. *J. Comput. Chem.* **1992**, **13**, 1011; b) A. Grossfield, WHAM: The Weighted Histogram Analysis Method, version 2.09, http://membrane.urmc.rochester.edu/wordpress/?page id=126.
34. Miyamoto, S.; Kollman, P. A. Settle: An analytical version of the SHAKE and RATTLE algorithm for rigid water models. *J. Comput. Chem.* **1992**, *13*, 952.
35. Mandado, M.; Hermida-Ramón, J. M. Electron density based partitioning scheme of interaction energies. *J. Chem. Theory Comput.* **2011**, *7*, 633.
36. Ramos-Berdullas, N.; Pérez-Juste, I.; Van Alsenoy, C.; Mandado, M. Theoretical study of the adsorption of aromatic units on carbon allotropes including explicit (empirical) DFT dispersion corrections and implicitly dispersion-corrected functionals: The pyridine case. *Phys. Chem. Chem. Phys.* **2015**, *17*, 575.
37. Frisch, M. J. et al. Gaussian 16 Revision C.01. 2016.
38. Cárdenas, G.; Lucia-Tamudo, J.; Mateo-delaFuente, H.; Palmisano, V. F.;Anguita-Ortiz, N.; Ruano, L.; Pérez-Barcia, A.; Díaz-Tendero, S.; Mandado, M.; Nogueira, J. J. MoBioTools: A Toolkit to Setup QM/MM Calculations. ChemRxiv 2022, doi: 10.26434/chemrxiv-2022-cncp2
39. Cárdenas, G. MoBioTools. 2022; https://github.com/mobiochem/MoBioTools.
40. Mandado, M.; Van Alsenoy, C. EDA-NCI: Energy Decomposition Analysis of Non-Covalent Interactions https://github.com/marcos-mandado/EDA-NCI
41. Pérez-Barcia, A.; Cárdenas, G.; Nogueira, J. J.; Mandado, M. Effect of the QM Size, Basis Set and Polarisation on QM/MM Energy Decomposition Analysis. ChemRxiv 2022, doi: 10.26434/chemrxiv-2022-8686w